New Concept of Gas Purification by Electron Attachment

Hajime Tamon, Hirotoshi Mizota, Noriaki Sano, Stefan Schulze, and Morio Okazaki
Dept. of Chemical Engineering, Kyoto University, Kyoto 606-01, Japan

A new concept of gas purification by electron attachment is proposed. Low-energy electrons generated in a corona-discharge reactor are captured by electronegative impurities, producing negative ions. The ions drift to the anode in the electric field and are removed at the anode of the reactor. Two types of reactors were used to remove the negative ions: a deposition-type reactor, which deposits negative ions at the anode surface; a sweep-out-type reactor, which sweeps out enriched electronegative impurities through the porous anode. Removals of dilute sulfur compounds, oxygen and iodine from nitrogen were conducted to verify the concept of gas purification. Simulation models were used to estimate removal efficiencies of these compounds, by taking into account electron attachment, and experimental constants of the models were determined. The removal efficiency correlated by the models agreed well with the experimental one.

Introduction

Gas purification involves the removal of vapor-phase impurities from gas streams. Many methods for gas purification have been proposed, and the primary operation falls into one of the following three categories: (1) absorption into a liquid; (2) adsorption on a solid; (3) chemical conversion to another compound (Kohl and Riesenfeld, 1979). Also research works are still done for all of these processes to improve them. Recently, the public has become interested in the following types of gas purification: (1) removal of indoor air pollutants; (2) complete removal of dioxin from incineration plants; (3) complete removal of radioactive iodine compounds; (4) simultaneous removal of NOx and SOx in exhaust gases from cogeneration plants; (5) removal and decomposition of halocarbons; (6) ultrahigh purification of gas used for semiconductor industries. These process gases contain electronegative impurities such as sulfur compounds and halogen compounds. Hence, development of efficient methods for the ultrahigh purification is expected. In order to achieve this development, it is very important to propose a new concept of gas purification based on a knowledge of physics that has not yet been applied in the research field of gas separation.

Gas-discharge technology is one promising method of achieving such ultrahigh purification. This method has been used in ozonizers (Devins, 1956) and electrostatic precipitators (White, 1963; Ogawa, 1984; Löffler, 1988). It is also well known that high-energy electrons generated by gas discharge ionize a gas and induce a plasma. Masuda (1987, 1991) and Masuda et al. (1987) have proposed an air purifier using a pulse-corona-induced plasma or a surface-corona-induced plasma. Higher electron energies can be achieved by these technologies since higher electric fields are allowed in pulse-corona and surface-corona systems than in direct-current systems because of the breakdown limits of the discharge. In the plasma region, electrons having oxidizing radicals (O, O^*, OH, O_2^*) and reducing radicals (NH, NH_2, N_2^*, N^*, H_2^*, H^*) are generated from the wet air or air containing ammonia. Air pollutants react with the active radicals, and gas purification is possible by converting them to a solid particulate (e.g., Hg-vapor to HgO), to a liquid (such as SO_2 to SO_3 or H_2SO_4), or to a gas (NO to NO_2). These conversions are also achieved by an electron beam (Kawamura, 1989). An economic assessment comparing the initial and continuing costs of the conventional chemical process for $DeNOx$ and $DeSOx$ (ammonia catalytic process for $DeNOx$ and calcium-gypsum scrubber for $DeSOx$) to the electron-beam process and the pulse-corona-induced plasma chemical process (PPCP) showed that PPCP is the most cost-effective of the three processes (Japan Association, 1991). However, low-energy electrons have not yet been used for gas purification.

When low-energy electrons collide with gas molecules, some of them are captured by gas molecules, and negative ions are produced. This phenomenon is called "electron attachment" (Massay, 1976). Electron attachment depends on electron energy, the structure of the gas molecule, and its

electron affinity. There is a large difference in the attachment probability of gas molecules, and this high selectivity is observed in the production of negative ions (Massay, 1976, 1979; Caledonia, 1975). Therefore, electronegative impurities of very low concentration become negative ions by electron attachment, and they can be separated from the neutral gas in an electric field. Tamon et al. (1989) constructed two kinds of separation equipment using a photocathode and glow discharge as electron sources. They reported the possible usefulness of this separation method by measuring the separation efficiency of sulfur hexafluoride (SF_6) from nitrogen (N_2). They found that the removal efficiency was high at a very low concentration of SF_6.

Since in most cases the process gas contains highly electronegative impurities, electron attachment seems to be the most effective way to remove them in an electric field. The purpose of our work is to establish a method of gas purification by electron attachment. In this article, we propose the concept of gas purification using low-energy electrons generated by corona discharge, and study the possibility that gas purification is achieved based on this concept. Then we present two types of corona-discharge reactors, and remove sulfur compounds, iodine (I_2), and oxygen (O_2) from N_2 as the first step of the research. We also discuss the purification mechanism, and try to correlate the removal efficiency based on simulation models.

Principle of Gas Purification

Figure 1 illustrates the principle of gas purification. High voltage is applied in a cylindrical reactor. The piano wire stretched at the center of reactor is a cathode, and the outer cylinder is an anode. The electrons are produced by corona discharge. During their drift to the anode in the electric field a part of them collides with gas molecules, and negative ions are produced by electron attachment.

For example, electron attachment to SF_6 is given as follows (Hickam and Fox, 1956). SF_6^- is produced by the impact of electrons with nearly zero energy:

$$SF_6 + e \rightarrow SF_6^- . \tag{1}$$

When electron energy increases, SF_5^- is formed according to Eq. 2:

$$SF_6 + e \rightarrow SF_5^- + F. \tag{2}$$

SF_6^- and SF_5^- also drift from the cathode to the anode, just as the electrons do. Because of this process the concentration of electronegative component at the anode is higher than that in the central part of the reactor. It is therefore very important to know how to remove the component at the anode.

We propose two ideas of corona-discharge reactors to remove negative ions at the anode as shown in Figure 2: (1) a deposition-type reactor, and (2) a sweep-out-type reactor. In the deposition-type reactor the negative ions adhere to the anode surface after they lose electrons there. The deposition-type reactor is not effective in removing electronegative impurities not deposited by the negative ions at the anode surface. Thus, we have proposed the sweep-out-type reactor. The anode of this reactor is a porous pipe made of sintered metal. A certain amount of gas is swept out through this pipe to remove the enriched electronegative component.

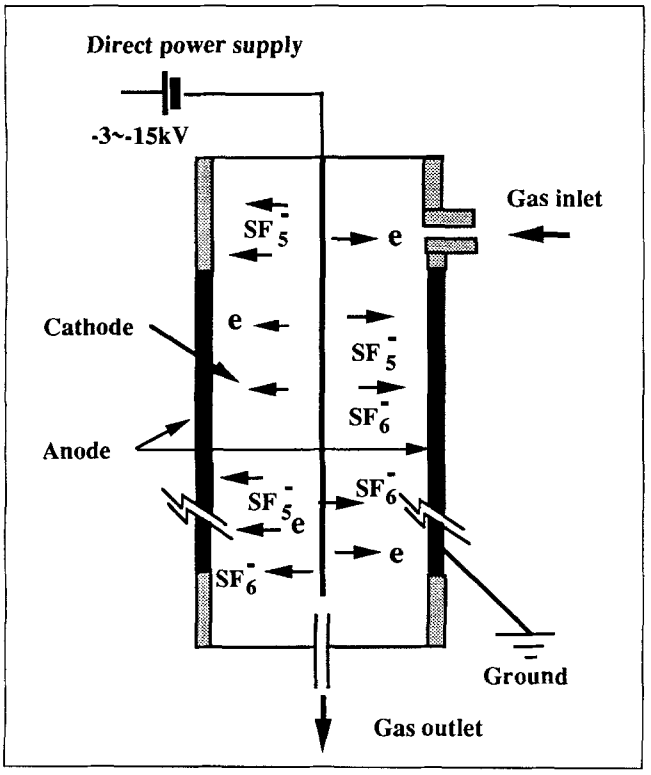

Figure 1. Principle of gas purification.

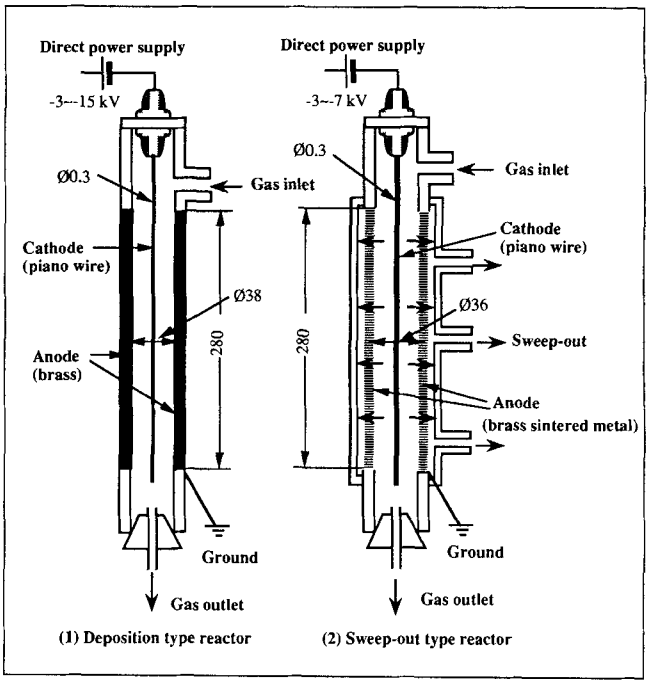

Figure 2. Equipment ideas of corona discharge reactor.
(1) Deposition-type reactor. (2) Sweep-out-type reactor.

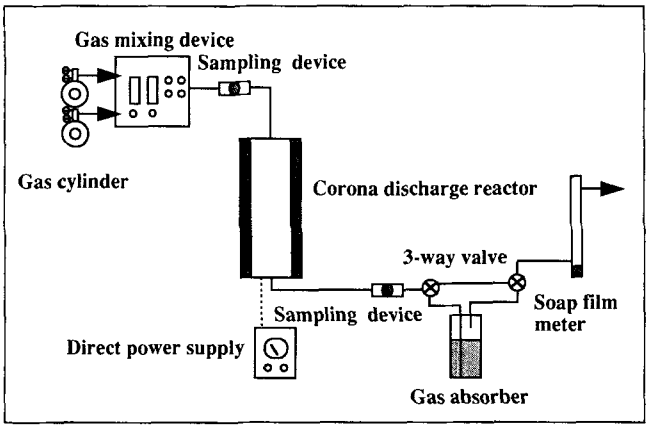

Figure 3. Experimental apparatus.

Gas Purification by Deposition-type Reactor

Experimental studies

Figure 3 shows a schematic diagram of the experimental apparatus. A sulfur compound was mixed with N_2 in a gas mixing device (Kojima Manufacturing Co. Ltd., KOFLOC GM-2A) and was then fed to a corona-discharge reactor. Sulfur hexafluoride (SF_6), dimethyl sulfide ($(CH_3)_2S$), carbonyl sulfide (COS), hydrogen sulfide (H_2S), methyl mercaptan (CH_3SH), carbon disulfide (CS_2), and sulfur dioxide (SO_2) were used as sulfur compounds. The reactor was connected to a direct power supply (Nichicon Co., DCG-50k2T). The gas flow rate was measured by a soap film meter.

Concentrations of sulfur compounds at the inlet and the outlet of the reactor were determined by a gas chromatograph (Shimadzu Corporation, GC-7A) with a flame photometric detector (FPD). A gas chromatograph (Yanagimoto Mfg. Co., Ltd., G-2800) with an electron capture detector (ECD) was used to measure the very low concentration of SF_6. Fluorine (F) was absorbed into 0.1-N NaOH solution, and the concentration was measured by a UV-spectrometer (Shimadzu Corporation, UV-260) according to the method proposed by Murakami (1982).

A detailed drawing of the reactor is shown in Figure 2. The cathode is a piano wire whose diameter is 0.3 mm, and the anode is a brass pipe whose inner diameter and length are 38 mm and 280 mm, respectively. Direct power of -3 kV to -15 kV is applied to the reactor to induce corona discharge. Negative ions are formed by electron attachment in the reactor. The ions drift to the anode in an electric field and deposit at the anode surface.

The removal ratio Ψ is defined by the following equation.

$$\Psi = (C_{A0} - C_{A1})/C_{A0} \tag{3}$$

where C_{A0} and C_{A1} are the inlet and outlet concentrations of the reactor. The removal ratio was experimentally determined under various conditions of inlet concentrations, corona discharge currents, and gas flow rates.

Removal of SF_6 from N_2

Figure 4 shows the removal efficiency of SF_6 from N_2 at various inlet concentrations of the reactor. The gas flow rate

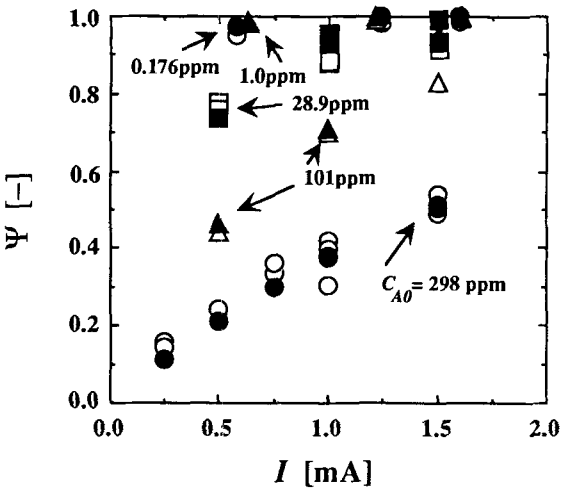

Figure 4. Removal efficiency of SF_6 from N_2: SV=18.9 h^{-1}.

Open symbol, measured; filled symbol, correlated.

Q_0 was around 1.67×10^{-6} m^3/s, and an atmospheric pressure was used in the reactor for all experiments. The abscissa is a discharge current, I, and the ordinate is the removal ratio Ψ defined by Eq. 3. It is found that Ψ is better the higher I is, because the probability of electron attachment increases with the number of electrons colliding with SF_6.

It can be seen that Ψ increases as C_{A0} decreases. For example, when C_{A0} is 1 ppm or 176 ppb, about 99% of SF_6 are removed from the reactor. Consequently, if sufficient electrons compared with electronegative gas molecules are supplied to the reactor, the removal efficiency improves.

The influence of gas flow rate, Q_0, on the removal ratio Ψ of SF_6 in N_2 is given in Figure 5. Inlet concentrations C_{A0} are 300 ppm and 1.05 ppm, and the corona discharge current I is 1.2 mA. It can be seen that Ψ decreases as Q_0 increases. When the space velocity (SV) is 163 h^{-1}, only 10% of SF_6 molecules are removed at 300 ppm. On the other hand, about

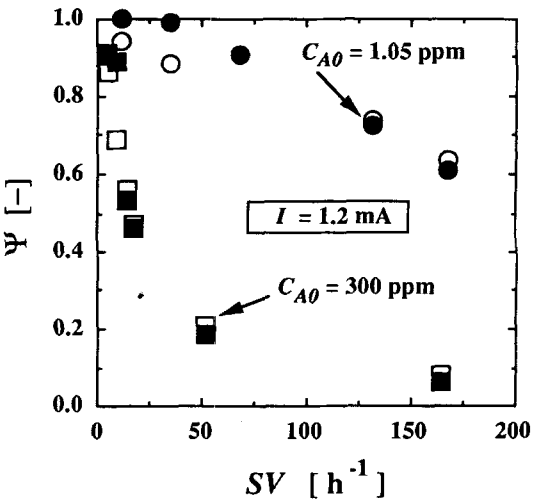

Figure 5. Influence of gas flow rate on removal efficiency of SF_6.

Open symbol, measured; filled symbol, correlated.

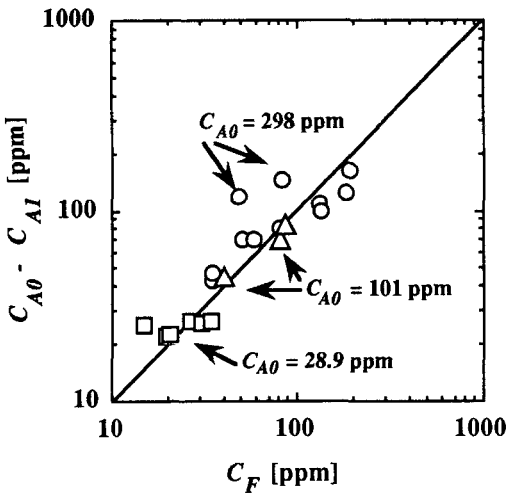

Figure 6. Relation of outlet concentration of fluorine C_F and $C_{A0}-C_{A1}$.

65% of SF_6 molecules are removed at 1.05 ppm. One can see that the removal of SF_6 is mainly influenced by the ratio of the number of electrons to the SF_6 molecules.

Electron attachment to SF_6

Electron attachment to SF_6 takes place as shown in Eqs. 1 and 2 (Hickam and Fox, 1956). Reaction-rate constants of electron attachment depend on electron energy, and electron energy depends on the ratio of electric field strength, E, to pressure, p, or, E/p. Chain et al. (1962) have reported that electron energy depends on the value of E/p in N_2. Therefore the rate constant in Eq. 1 or Eq. 2 is a function of E/p. The distribution of E/p in the present reactor was calculated, and the distribution of electron energy was also estimated. The estimated result shows that electron energy in the reactor is more than 0.3 eV. Hickam and Fox (1956) have reported the variation in the electron energy of the yield of SF_6^- and SF_5^- by electron impact in SF_6, and shown that SF_5^- is the main ion in case that electron energy is more than 0.3 eV. It can thus be seen that the dissociative attachment given by Eq. 2 takes place in the present reactor.

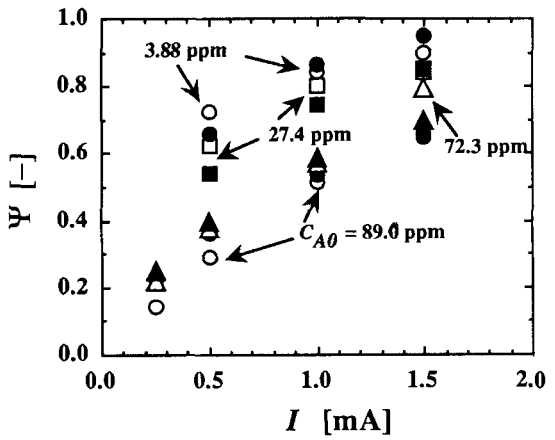

Figure 7. Removal efficiency of $(CH_3)_2S$ from N_2:SV = 18.9 h^{-1}.

Open symbol, measured; filled symbol, correlated.

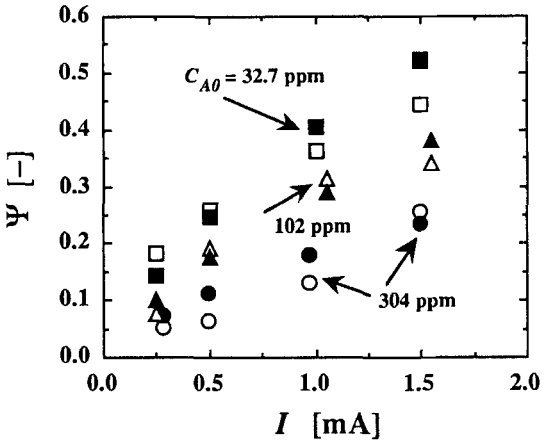

Figure 8. Removal efficiency of SO_2 from N_2:SV = 18.9 h^{-1}.

Open symbol, measured; filled symbol, correlated.

In order to verify that the electron attachment reaction is expressed by Eq. 2 in the present reactor, the analysis of F at the outlet of the reactor was carried out. Figure 6 gives the relation of C_F at the reactor outlet and the value of $C_{A0}-C_{A1}$, which means the concentration of the F atom produced by Eq. 2. Since F produced in the reactor repeatedly deposits and desorbs at the anode surface, the measured values of C_F are scattered. The concentration of F, however, almost agrees with the one calculated from the inlet and outlet concentrations of SF_6. This result also indicates that the dissociative attachment given by Eq. 2 occurs in the reactor and SF_5^- deposits at the anode surface.

Removal of other sulfur compounds from N_2

We conducted removal experiments of $(CH_3)_2S$, SO_2, CH_3SH, CS_2, COS, and H_2S at several inlet concentrations and gas flow rates. Examples of the experimental results are shown in Figures 7 and 8. These figures indicate that Ψ increases with I and becomes high as C_{A0} decreases. Similar removal behaviors for other sulfur compounds were observed. The values of SV for our removal experiments are shown in Table 1. On the other hand, the values of SV for the real plants have been reported as follows (Kohl and Riesenfeld, 1979): 13.3 h^{-1} for SO_2 removal by the magnesium oxide scrubbing; $90 \sim 419$ h^{-1} for SO_2 removal by a Cominco process absorber; $5.38 \sim 37.4$ h^{-1} for H_2S removal by the iron oxide purifier; and $81 \sim 92$ h^{-1} for the removal of organic sulfur by the soda-iron plant. The practicality of SV can be seen in the present work.

If reaction by-products are generated by electron attachment and are hazardous, we should remove them by conventional methods such as absorption and adsorption. It is very important to identify by-products generated in the reactor. In this work, no by-products were observed in the removal of $(CH_3)_2S$, SO_2, H_2S, COS, and CS_2. Some by-product, which was thought to be produced by a dissociative attachment reaction, was detected by a gas chromatograph in the removal of CH_3SH. Although it hasn't been identified yet, its concentration seems to be very low, because the chromatogram shows its peak area to be much smaller than that of CH_3SH.

The experimental results indicate that the order of re-

Table 1. Correlating Results for Experimental Data

Comp.	Neg. Ion	Parameters [$m^3 \cdot mol^{-1} \cdot s^{-1}$] k_1	$\mu_e k_2/\mu_{B^-}$	Space vel. SV [h^{-1}]	Std. Dev.
SF_6	SF_5^-	9.83×10^9	8.79×10^9	4.67 ~ 163	0.045
CH_3SH	S^-	6.00×10^9	7.65×10^9	11.5 ~ 64.1	0.094
SO_2	S^-	8.34×10^8	9.99×10^{10}	8.96 ~ 212	0.069
CS_2	S^-	6.04×10^9	8.25×10^{10}	3.67 ~ 185	0.106
COS	S^-	2.62×10^9	0	4.67 ~ 169	0.100
H_2S	S^-	1.75×10^{10}	3.36×10^9	4.70 ~ 28.5	0.076
$(CH_3)_2S$	S^-	3.91×10^9	1.48×10^{10}	8.56 ~ 69.0	0.086

moval efficiency is $H_2S > SF_6 > CH_3SH > (CH_3)_2S > CS_2 > COS > SO_2$. The removal efficiency of sulfur compounds in N_2 is high at low C_{A0}, large I, and small Q_0. It can be concluded therefore that the present method can remove the sulfur compounds. Since oxygen and moisture often coexist in the actual process, we report their influence on removal efficiency in a subsequent article.

Analysis of used anode by EPMA

In order to investigate the removal mechanism of sulfur compounds in the reactor, it is important to understand the deposition of negative ions at the anode surface. The distribution of sulfur on the anode surface used to remove sulfur compounds was measured by an electron probe microanalysis (EPMA). An X-ray microanalyzer (Horiba, Ltd., EMAX-2200S) was used for this analysis. Figure 9 shows a scanning electron microscope (SEM) image of the anode surface

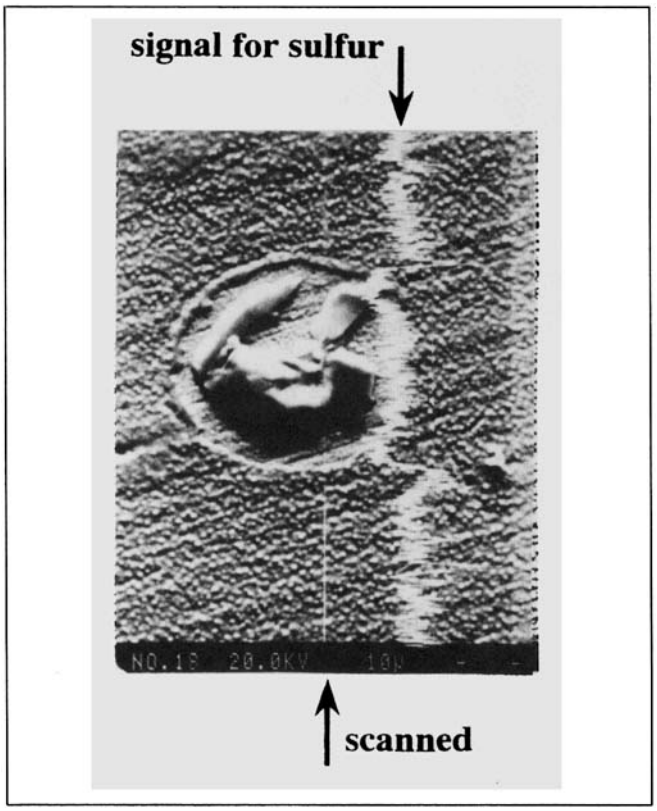

Figure 9. Distribution of sulfur on anode surface by EPMA.

(Hitachi, Ltd., S-510). The wavy white line indicates the distribution of sulfur scanned along the white straight line, showing that sulfur atoms uniformly distribute on the anode surface.

Simulation of removal efficiency of sulfur compounds

The electron attachment reaction and the transport mechanism of electrons and negative ions in an electric field are modeled to correlate the removal ratio of sulfur compounds in N_2. Typical electron attachments are dissociative, dielectric, radiative, and three-body (Massay, 1976). Dissociative attachment has a larger reaction-rate constant than other attachments. Therefore the following reaction is considered in the present work:

$$A + e \underset{k_2}{\overset{k_1}{\rightleftarrows}} B^- + C \tag{4}$$

Negative ions produced by this reaction are shown in Table 1. Although a reaction by-product of F was generated from SF_6, F was not removed in the present reactor, as shown in Figure 6. In the removal of other sulfur compounds, no reaction by-products were observed with the exception of a by-product of CH_3SH, which was also considered to be negligibly small. Consequently, we have neglected side reactions in this work. The reaction rate is given by Eq. 5.

$$R_A = dC_A/dt = -(k_1 C_A C_e - k_2 C_C C_{B^-}). \tag{5}$$

In this work, we use the following assumptions to correlate the removal ratio of sulfur compounds in a steady state:

1. A gas flows as a piston flow in the reactor.
2. Electrons and negative ions transfer to the anode by drifting in the electric field.
3. Reaction-rate constants, the mobility of electrons, and the mobility of negative ions are kept constant regardless to the electric field strength.
4. All negative ions produced by electron attachment deposit at the anode surface.

Although the gas flow is laminar in the reactor because of the low Reynolds number, we have assumed a piston flow. In a corona-discharge reactor, ionized gas molecules induce a gas convection, the so-called "ion wind" or "corona wind" (Yabe et al., 1978; Yamamoto and Velkoff, 1981; Löffler, 1988). The corona wind has been studied several times to estimate its influence on the efficiency of the electrostatic precipitator because the wind disturbs dust collection, and is considered to be 1.5 ~ 2.0 m/s (Yabe et al., 1978). Even if the gas flow is laminar in the reactor, the wind trends to flatten the gas velocity profile and to reduce the thickness of the boundary layer on the anode. Since a corona wind of 1.5 ~ 2.0 m/s takes place in the radial direction of the reactor, the reactor is considered to be perfectly mixed in the radial direction.

It has been reported that the reaction-rate constant of electron attachment depends on the electric field strength (Massay, 1976). However, dependency on various sulfur compounds has not been reported in the literature. We have adopted the preceding assumption as the first approximation.

In the future, we should simulate the removal efficiency of sulfur compounds by taking the dependency into account.

A mass balance equation for an electron in the radial direction is given by Eq. 6:

$$(1/r)d(rN_{er})/dr = R_A. \tag{6}$$

In Eq. 6 N_{er} is a molar flux of electron, and is expressed by Eq. 7.

$$N_{er} = C_e v_e = C_e \mu_e E. \tag{7}$$

The electric field strength E is as follows:

$$E = V/\{r \ln(R/R_0)\}. \tag{8}$$

From Eqs. 5, 6, 7 and 8,

$$[\mu_e V/\{r \ln (R/R_0)\}]dC_e/dr = -(k_1 C_A C_e - k_2 C_C C_{B^-}). \tag{9}$$

As for negative ion B^-, the following equation is derived by a charge balance:

$$C_{B^-} = (\mu_e/\mu_{B^-})(C_{e0} - C_e) \tag{10}$$

The mass balance of components A and C in the axial direction of the reactor give Eqs. 11 and 12:

$$Q_0 dC_A/dz = -2\pi \int_{R_0}^{R} r(k_1 C_A C_e - k_2 C_C C_{B^-})\, dr \tag{11}$$

$$Q_0 dC_C/dz = 2\pi \int_{R_0}^{R} r(k_1 C_A C_e - k_2 C_C C_{B^-})dr. \tag{12}$$

The boundary conditions are given as follows. At the reactor inlet,

$$C_A = C_{A0}, \quad C_{B^-} = 0, \quad C_C = 0 \quad \text{at} \quad z = 0. \tag{13}$$

At the cathode surface,

$$C_{B^-} = 0, \quad C_C = 0, \quad C_e = C_{e0} \quad \text{at} \quad r = R_0 \tag{14}$$

where C_{e0} is given by Eq. 15.

$$C_{e0} = N_{e0}/v_{e0} = N_{e0}/(\mu_e E_0). \tag{15}$$

The electron flux at the cathode surface, N_{e0}, is

$$N_{e0} = I/(2\pi R_0 Z Q_{el} N_{AV}). \tag{16}$$

In Eq. 8, E_0 is the electric field strength at $r = R_0$. Accordingly, C_{e0} in Eq. 14 becomes

$$C_{e0} = I \ln (R/R_0)/(2\pi Z \mu_e V Q_{el} N_{AV}). \tag{17}$$

The removal ratio can be estimated by solving Eqs. 9 to 12 under the boundary conditions Eqs. 13 and 14. It is convenient to introduce the following dimensionless variables to the fundamental equations:

$$x^2 = (r^2 - R_0^2)/(R^2 - R_0^2); \qquad y = z/Z;$$

$$\alpha = C_{A0} k_1 (R^2 - R_0^2) \ln (R/R_0)/(\mu_e V);$$

$$\beta = \pi k_1 C_{e0} Z(R^2 - R_0^2)/Q_0 = k_1 C_{e0} Z/v_z; \qquad \zeta = k_2/k_1;$$

$$\kappa = C_C/C_{A0}; \qquad \sigma = \mu_e/\mu_{B^-}; \qquad \phi = C_{B^-}/C_{e0};$$

$$\psi = 1 - C_A/C_{A0}; \qquad \omega = C_e/C_{e0}. \tag{18}$$

These dimensionless variables are inserted into Eqs. 9 and 10 to derive the following equations:

$$d\omega/dx = -\alpha x\{(1-\psi)\omega - \zeta\kappa\phi\} \tag{19}$$

$$\phi = \sigma(1-\omega). \tag{20}$$

Equation 20 is inserted into Eq. 19, and the following equation is obtained by integrating Eq. 19 under Eq. 14 because ψ and κ are constant in the radial direction of the reactor, according to the assumption

$$\omega = \zeta\kappa\sigma/(1-\psi+\zeta\kappa\sigma) + \{(1-\psi)/(1-\psi+\zeta\kappa\sigma)\} \times \exp\{-\alpha(1-\psi+\zeta\kappa\sigma)x^2/2\}. \tag{21}$$

Equations 11 and 12 become Eqs. 22 and 23 by using the dimensionless variables:

$$d\psi/dy = 2\beta \int_0^1 \{(1-\psi)\omega - \zeta\kappa\phi\} x\, dx \tag{22}$$

$$d\kappa/dy = 2\beta \int_0^1 \{(1-\psi)\omega - \zeta\kappa\phi\} x\, dx. \tag{23}$$

From Eqs. 22 and 23,

$$\kappa = \psi. \tag{24}$$

Inserting Eqs. 20, 21 and 24 into Eq. 22, and integrating the obtained equation, the following equation is derived:

$$d\psi/dy = [2\beta(1-\psi)/\{\alpha(1-\psi+\sigma\zeta\psi)\}] \times [1 - \exp\{-\alpha(1-\psi+\sigma\zeta\psi)/2\}]. \tag{25}$$

Equation 13 becomes Eq. 26.

$$\psi = 0 \quad \text{at} \quad y = 0. \tag{26}$$

Equation 25 can be numerically solved by using the Runge-Kutta method. The value of ψ at $y = 1$ is defined as the removal ratio Ψ according to Eq. 3. In calculating the removal ratio, the rate constants for electron attachment and the mobility of negative ions are unknown. Therefore, an optimization program, which is the Marquardt method, was used to determine k_1 and $\mu_e k_2/\mu_{B^-}$. Although electron attachment reactions are reported in the literature (Caledonia, 1975; Massay, 1976), attachment to sulfur compounds has not been

verified, except in SF_6. In the present work, SF_5^- and S^- are regarded as the negative ions produced by electron attachment, as shown in Table 1.

Parameters k_1 and $\mu_e k_2/\mu_{B^-}$ have been determined by adjusting the parameters for all experimental results under various conditions of different inlet concentrations, discharge currents, and gas flow rates, and are listed in Table 1. The standard deviations of the correlated results from the experimental ones are also shown in Table 1.

As seen in Table 1, the parameters $k_1 = 9.83 \times 10^9$ $m^3 \cdot mol^{-1} \cdot s^{-1}$ and $\mu_e k_2/\mu_{B^-} = 8.79 \times 10^9$ $m^3 \cdot mol^{-1} \cdot s^{-1}$ have been determined in the removal of SF_6. These results seem to be reasonable when compared them with other results. Fehsenfeld (1970) has reported $k_1 = 1.32 \times 10^{11}$ $m^3 \cdot mol^{-1} \cdot s^{-1}$ by an afterglow method. The reported rate constant is considered to be large because the electron energy in this method is very low. On the other hand, Ayala (1981) has reported $k_1 = 3.25 \times 10^{10}$ $m^3 \cdot mol^{-1} \cdot s^{-1}$ by a pulse-sampling method, in which electron energy is larger than that in an afterglow method. Since the energy is less than that in corona discharge, the rate constant reported by Ayala (1981) is a little bit larger than that in the present work.

Figures 4 and 5 compare the correlated removal ratio of SF_6 and the measured one. Open symbols mark the measured removal ratios, while filled symbols mark the correlated ones. The correlated results fit very well with the experimental results. Figures 7 and 8 show the examples of correlated results for $(CH_3)_2S$ and SO_2. A similar correlation was obtained for H_2S, CH_3SH, CS_2, and COS. The parameters ascertained are shown in Table 1. Table 1 also shows that the values of k_1 for $(CH_3)_2S$ and SO_2 are 3.91×10^9 and 8.34×10^8 $m^3 \cdot mol^{-1} \cdot s^{-1}$, and Figures 7 and 8 show that Ψ of $(CH_3)_2S$ is about twice that of SO_2. If electronegative impurities have these different rate constants, they seem to be differentiated by the present method. As seen from these figures and Table 1, the influence of the concentration of gas at the inlet, discharge current, and gas flow rate on the removal efficiency can be evaluated by the proposed model.

Although the agreement of correlated results and experimental ones suggests that SF_5^- or S^- is produced in the reactor, this is no more than an indirect confirmation of electron attachment. A more sophisticated investigation for the attachment mechanism will be needed in the future. We should also study the feasibility of the present method by comparing its initial and continuing costs with the costs of conventional methods for gas purification.

Gas Purification by Sweep-out-type Reactor

Experimental studies

Figure 10 shows a schematic diagram of an experimental apparatus for O_2 removal. The apparatus is placed in a box, and leakage of O_2 from the room air is prevented by feeding N_2 to the box. Figure 11 shows a schematic diagram for I_2 removal. I_2 sublimates in a temperature-controlled bath, and is mixed with N_2. Teflon tubes and connections are used instead of metal ones to prevent I_2 from reacting with the metal surface in the apparatus.

Concentrations of O_2 at the inlet and the outlet of the reactor were determined by an oxygen analyzer (Toray Industries, Inc., LC-700). I_2 was absorbed into a KI solution (2×10^{-4} mol/m^3), and the concentration was measured by a UV-spectrometer (Shimadzu Corp., UV-260) according to the method proposed by Adachi et al. (1971).

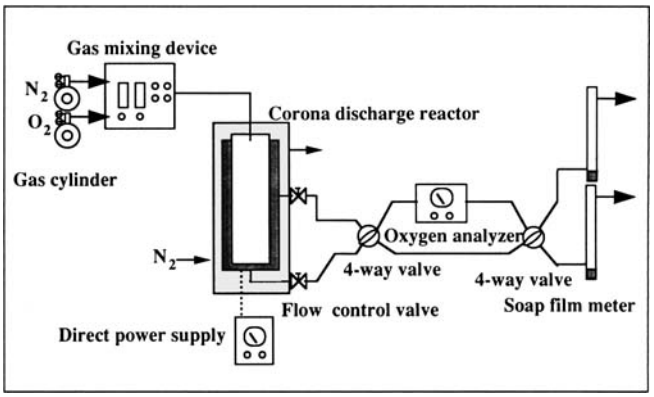

Figure 10. Experimental apparatus for O_2 removal.

A detailed drawing of the reactor is shown in Figure 2. The inner piano wire, whose diameter was 0.3 mm, was used as the cathode, and the anode was a brass porous pipe whose inner diameter was 36 mm and length was 280 mm, respectively. The anode was made of sintered metal, whose pore diameter was 1.0 μm and porosity was 38%. Direct power of -3 kV to -7 kV was applied to the reactor to produce low-energy electrons. Negative ions were produced by the electron attachment to O_2 or I_2. The ions drifted to the anode, and a portion of the negative ions adhered there. Other ions became neutral molecules after they lost electrons there. The enriched neutral molecules were swept out through the porous anode. Since the concentration of electronegative component at the anode was higher than that in the center of the reactor, back diffusion of the component occured from the anode to the central part of reactor. Because corona wind takes place in the reactor, the boundary layer on the anode surface was very thin, and the back diffusion rate large. It is therefore very important to choose an adequate sweep-out rate to prevent back diffusion.

Removal of O_2 and I_2 from N_2

Figure 12 shows the removal efficiency of O_2 from N_2 at some gas flow rates. The corona discharge current, I, is 1.5 mA. It can be seen that Ψ, defined by Eq. 3, increases with

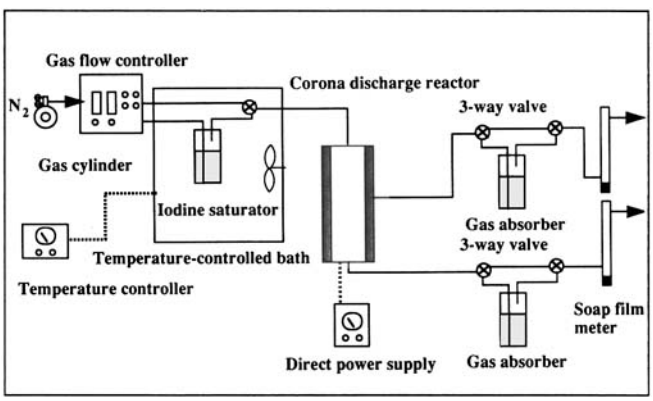

Figure 11. Experimental apparatus for I_2 removal.

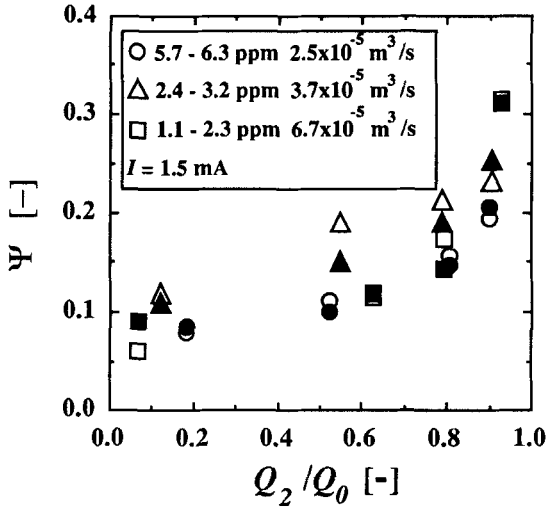

Figure 12. Removal efficiency of O_2 from N_2 by sweep-out-type reactor.

Open symbol, measured; filled symbol, correlated.

Q_2/Q_0. The removal efficiency of I_2 is shown in Figure 13. I_2 removal gives a similar tendency to O_2 removal. A part of negative ions drifting to the anode adheres there, and other ions are swept out or diffused back to the center of the reactor. Hence, it is impossible to distinguish the sweep-out effect from the experimental results. It is necessary to estimate the sweep-out effect by using the simulation model described later.

Simulation of removal efficiency

The following simple reaction simulates the efficient removal of O_2 or I_2 in this work:

$$A + e \xrightarrow{k_1} A^- . \tag{27}$$

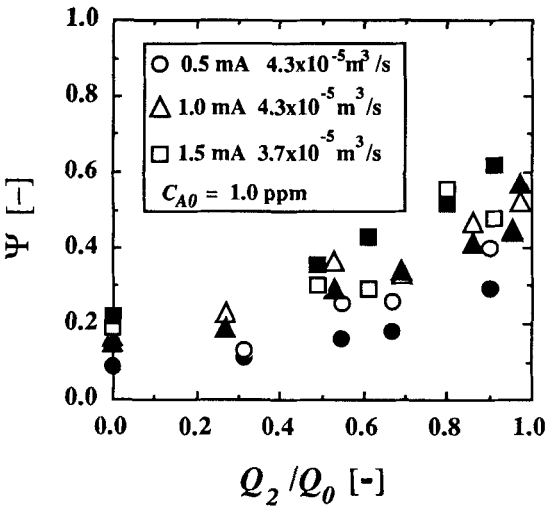

Figure 13. Removal efficiency of I_2 from N_2 by sweep-out-type reactor.

Open symbol, measured; filled symbol, correlated.

The reaction rate is given by Eq. 28:

$$R_A = dC_A/dt = -k_1 C_A C_e . \tag{28}$$

The following assumptions are adopted in addition to Assumptions 1 to 3 used in the deposition-type reactor:

5. A portion of the negative ions produced by electron attachment adheres to the anode surface, and the probability of deposition is defined as an accommodation coefficient a. The value of a is the ratio of the molecules deposited at the anode to the colliding ones.

6. The sweep-out rate per unit anode area is kept constant along the reactor.

The mass balance equation of an electron in the radial direction is given by Eq. 6. From Eqs. 6, 7, 8 and 28, we get

$$\frac{\mu_e V}{r \ln\left(\frac{R}{R_0}\right)} \frac{dC_e}{dr} = -k_1 C_A C_e . \tag{29}$$

Because C_A is constant in the radial direction of the reactor according to the assumption, Eq. 29 can be solved by Eq. 14:

$$\frac{C_e}{C_{e0}} = \exp\left[-\frac{k_1 C_A (r^2 - R_0^2) \ln\left(\frac{R}{R_0}\right)}{2\mu_e V} \right]. \tag{30}$$

The molar flux of A in the boundary layer N'_A can be estimated as follows:

$$d(rN'_A)/dr = 0 \tag{31}$$

$$N'_A = -DdC'_A/dr + v_s C'_A \tag{32}$$

where v_s is the sweep-out velocity and is given by Eq. 33:

$$v_s = Q_2/(2\pi rZ). \tag{33}$$

The boundary conditions are given by the following equations:

$$C'_A = C_A \quad \text{at} \quad r = R - \delta \tag{34}$$

$$C'_A = C_{A2} \quad \text{at} \quad r = R. \tag{35}$$

The concentration profile of A, C'_A, can be obtained by solving Eqs. 31 to 33 under Eqs. 34 and 35. Then the molar flux of A at the anode surface N'_{AR} is given by Eq. 36:

$$N'_{AR} = \frac{1}{R} \frac{\frac{Q_2}{2\pi Z}\left[C_A \left(\frac{R}{R-\delta}\right)^{Q_2/(2\pi ZD)} - C_{A2} \right]}{1 - \left(\frac{R}{R-\delta}\right)^{Q_2/(2\pi ZD)}}. \tag{36}$$

The relation of C_A and C_{A2} is derived from the mass bal-

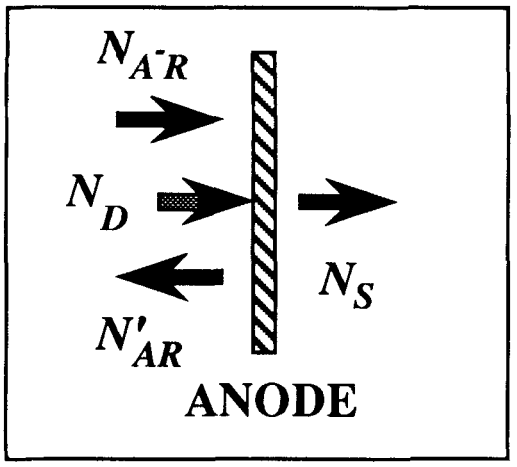

Figure 14. Mass balance in boundary layer.

ance at the anode surface shown in Figure 14. The mass balance at the anode surface is given by Eq. 37:

$$N_{A^-R} = N'_{AR} + N_S + N_D \tag{37}$$

where the molar flux of negative ion N_{A^-R} is the following:

$$N_{A^-R} = \frac{\mu_e(C_{e0} - C_{e2})V}{R \ln \dfrac{R}{R_0}}. \tag{38}$$

The molar flux of component A, N_S, is swept out through the anode and is given by the following equation:

$$N_S = C_{A2}Q_2/(2\pi RZ). \tag{39}$$

In Eq. 37 N_D is the disappearing molar flux at the anode surface by deposition of negative ions and is given by Eq. 40 using the accommodation coefficient a:

$$N_D = aN_{A^-R}. \tag{40}$$

The following equation is derived by inserting Eqs. 36 and 38–40 into Eq. 37:

$$C_A - C_{A2} = (1-a)\frac{2\pi Z\mu_e(C_{e0} - C_{e2})V}{Q_2 \ln (R/R_0)} \times \left[\frac{1}{\left(\dfrac{R}{R-\delta}\right)^{Q_2/(2\pi ZD)}} - 1\right]. \tag{41}$$

Equation 42 is derived by the mass balance of components A in the axial direction of the reactor:

$$d(QC_A)/dz = -Q_2C_{A2}/Z - 2\pi RN_D. \tag{42}$$

Since the sweep-out rate per unit anode area is constant, the flow rate Q at an arbitrary position in the axial direction of reactor becomes

$$Q = Q_0 - zQ_2/Z. \tag{43}$$

By inserting Eqs. 40 and 43 into Eq. 42,

$$\left(Q_0 - \frac{z}{Z}Q_2\right)\frac{dC_A}{dz} = \frac{Q_2}{Z}(C_A - C_{A2}) - 2\pi a\frac{\mu_e(C_{e0} - C_{e2})V}{\ln (R/R_0)}. \tag{44}$$

Also, C_A can be determined by solving Eqs. 41 and 44. Here it is convenient to introduce the dimensionless variables defined in Eqs. 18 and 45 to these equations:

$$\gamma = 1 - \frac{1}{1 - \left(\dfrac{R}{R-\delta}\right)^{Q_2/(2\pi ZD)}}; \qquad \eta = Q_2/Q_0. \tag{45}$$

These dimensionless variables are inserted into Eqs. 41 and 44, and the following equation is derived:

$$\frac{d\psi}{dy} = \frac{\dfrac{2\beta}{\alpha}\{1 - \exp[-\alpha(1-\psi)/2]\}(1 - a + \gamma a)}{\gamma(1 - y\eta)}. \tag{46}$$

Equation 46 can be solved using the boundary condition Eq. 26. The value of ψ at $y = 1$ is Ψ according to Eq. 3, and Ψ is given by Eq. 47:

$$\Psi = 1 - \frac{2}{\alpha}\ln\{1 + [\exp(\alpha/2) - 1](1-\eta)^{[\beta(1-a+a\gamma)]/(\eta\gamma)}\}. \tag{47}$$

In the correlation of the removal ratio, Ψ, the rate constant of electron attachment, k_1, the thickness of boundary layer, δ, and the accommodation coefficient, a, are unknown. The value of diffusion coefficient D was predicted by the Chapman-Enskog formulas (Chapman and Cowling, 1951; Hirschfelder et al., 1954). The values of k_1, a and δ are adjusted by the Marquardt method for all removal data. The values of k_1, δ and a are listed in Table 2. Standard deviations of the correlated results from the experimental ones and space velocities are also presented in Table 2. Comparison of the observed removal ratio and the correlated one is shown in Figures 12 and 13. It can be seen that the correlated removal ratio agrees with the one observed.

As described before, a wind of 1.5 ~ 2.0 m/s occurs in the radial direction of the reactor (Yabe et al., 1978), and the thickness of boundary layer δ on the anode is very thin. The

Table 2. Correlating Results for Experimental Data

Comp.	k_1 [$m^3 \cdot mol^{-1} \cdot s^{-1}$]	a	δ [m]	SV [h^{-1}]	Std. Dev.
O_2	2.13×10^{11}	0.03	8.12×10^{-5}	81.3 ~ 1255	0.025
I_2	4.40×10^{10}	0.20	8.12×10^{-5}	110 ~ 1145	0.175

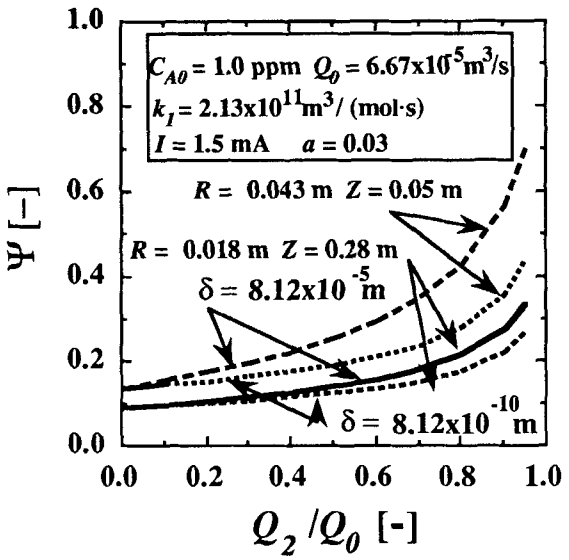

Figure 15. Sweep-out effect and influence of reactor shape on O_2 removal.

value of δ was determined from the heat transfer coefficient when hot air perpendicularly impinged on the plate. When the corona wind is 1.5 m/s, δ seems to be $5.6\times10^{-5}\sim2.2\times10^{-4}$ m. Accordingly, the value of δ determined in the present work is considered to be reasonable, as shown in Table 2.

Sweep-out effect

It is important to evaluate how the removal efficiency is improved by the sweep out. However, it is difficult to separate the sweep-out effect from the experimental results because the deposition of negative ions also takes place in the reactor. Therefore, we have studied the effect by using the proposed model. In order to obtain the removal ratio when the sweep-out effect is negligibly small, the simulation was also carried out under conditions where δ is very thin and

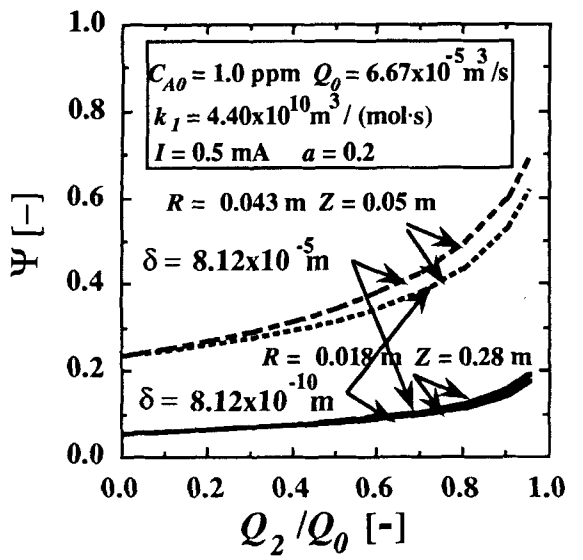

Figure 16. Sweep-out effect and influence of reactor shape on I_2 removal.

that back-diffusion is controlling. Here the electronegative component is removed solely by the deposition of negative ions. We can evaluate the sweep-out effect by comparing the two simulation results.

Figures 15 and 16 show the sweep-out effect in the removal of O_2 and I_2. The solid lines indicate the results simulated using the parameters listed in Table 2, while the dotted lines show the simulation results when it is assumed that δ is very thin. The difference between the solid and dotted lines is considered to be the sweep-out effect. When the sweep-out rate increases, the difference increases and the sweep-out helps increase the removal efficiency. Figures 15 and 16 show that the sweep-out effect for O_2 removal is larger than that for I_2.

Table 2 shows that k_1 for O_2 is larger than that for I_2, and that a for I_2 is larger than that for O_2. Since the negative ion of O_2 is more than that of I_2, a large amount of negative ion becomes the neutral molecule at the anode surface in the O_2 removal. O_2 is easily removed by sweep-out compared with I_2. It is therefore concluded that the sweep-out-type reactor is effective in removing the electronegative impurity whose k_1 is large and a is small.

Conceptual design and reactor shape

Figures 15 and 16 also show that the reactor shape influences the removal efficiency of O_2 and I_2. In these figures, the solid lines indicate the simulated results for the corona-discharge reactor used in the present work, while the broken lines denote the simulated results in a different reactor shape ($R = 0.043$ m and $Z = 0.05$ m), whose reactor volume is the same as the one constructed in this work. The dotted lines in these figures are the simulated results for both reactor shapes when it is assumed that δ is very thin and that the back-diffusion is controlling. Here the applied voltage and the discharge current are assumed to be independent on the reactor shape. The short and flat reactor increases the removal ratio, intensifies the sweep-out effect, and is desirable for a sweep-out-type reactor. This is because the anode area becomes small and the sweep-out velocity becomes large as the reactor radius becomes large at the same reactor volume. Moreover, electron attachment is accelerated since the electron density per unit cathode length increases when the reactor length is reduced.

We proposed the sweep-out-type reactor, and tried to verify its design by the removal of O_2 and I_2 from N_2. The principle of the proposed reactor has been verified by the experiment and the simulation. However, the sweep-out effect is not large because a portion of the negative ions of O_2 and I_2 adheres to the anode surface. We feel that this type of reactor would be effective in removing the impurities not deposited by the negative ions. More detailed study will be needed in the future.

Conclusions

Negative ions are produced by electron attachment to gas molecules. In the present work, a new concept of gas purification based on electron attachment was proposed. Electrons were produced from a cathode in a corona-discharge reactor, and drifted to an anode in an electric field. Electrons were attached to electronegative impurities during their drift from the cathode to the anode, forming negative ions. The ions

drifting in the electric field adhered to the anode surface or were swept out through the porous anode.

In order to verify the proposed concept of gas purification, we constructed two types of corona-discharge reactors, and conducted removal experiments of dilute SF_6, $(CH_3)_2S$, COS, H_2S, CH_3SH, CS_2, SO_2, O_2, and I_2 from N_2. The removal efficiency increased with the discharge current, and decreased with the concentration of electronegative components. Consequently, it was found that a high removal efficiency was achieved if sufficient electrons compared with electronegative gas molecules were supplied to the reactor.

To estimate the removal efficiency in the deposition-type reactor and the sweep-out type reactor, simulation models were proposed by taking into account the electron attachment reaction and the transport mechanism of electrons and negative ions in the electric field. Experimental constants appearing in the models were determined from the experimental results by an optimization program. The correlated results by the proposed model agreed well with the experimental ones. It was found that the proposed models were useful in the design of corona-discharge reactors for gas purification.

Acknowledgment

Financial support was supplied by the Ministry of Education, Science and Culture of Japan for Grant-in-Aid on Development of Scientific Research, No. 01890006 (1989), and Priority-Area Research, No. 03202224 (1991). The authors are grateful to Tetsuji Yoneda, Shoji Nishida, Koji Fukada, and Takeshi Sakaitani for their assistance in the experimental work.

Notation

N_{AV} = Avogadro's number, mol^{-1}
Q_{el} = charge of one electron, C
R = radius of anode in reactor, m
R_0 = radius of cathode in reactor, m
r = coordinate along the radius of reactor, m
t = time, s
V = discharge voltage, V
v_e = velocity of electron, m/s
v_z = velocity of gas, m/s
Z = length of reactor, m
z = coordinate along the axis of reactor, m

Greek letters

μ_e = mobility of electron, $m^2 \cdot V^{-1} \cdot s^{-1}$
μ_{A^-} = mobility of negative ion, $m^2 \cdot V^{-1} \cdot s^{-1}$
μ_{B^-} = mobility of negative ion, $m^2 \cdot V^{-1} \cdot s^{-1}$

Literature Cited

Adachi, M., W. Eguchi, K. Kato, and T. Tohdo, "Partition Equilibria of Iodine in Air-Water System Containing Sodium Hydroxide," *Kagaku Kogaku*, **35**, 877 (1971).

Ayala, J. A., "Thermal Electron Attachment to CCl_4, $CHCl_3$, CH_2Cl_2 and SF_6," *J. Phys. Chem.*, **85**, 3989 (1981).

Caledonia, G. E., "A Survey of the Gas-Phase Negative Ion Kinetics of Inorganic Molecules. Electron Attachment Reactions," *Chem. Rev.*, **75**, 333 (1975).

Chain, L. W., A. V. Phelps, and M. A. Biondi, "Measurements of the Attachment of Low-Energy Electrons to Oxygen Molecules," *Phys. Rev.*, **128**, 219 (1962).

Chapman, S., and T. G. Cowling, *Mathematical Theory of Non-Uniform Gases*, 2nd ed., Cambridge Univ. Press, Cambridge, England (1951).

Devins, J. C., "Mechanism of Ozone Formation in the Silent Electric Discharge," *J. Electrochem. Soc.*, **103**, 460 (1956).

Fehsenfeld, F. C., "Electron Attachment to SF_6," *J. Chem. Phys.*, **53**, 2000 (1970).

Hickam, W. M., and R. E. Fox, "Electron Attachment in Sulfur Hexafluoride Using Monoenergetic Electron," *J. Chem. Phys.*, **25**, 642 (1956).

Hirschfelder, J. O., C. F. Curtiss, and R. B. Bird, *Molecular Theory of Gases and Liquids*, Wiley, New York, p. 539 (1954).

Japan Association for Mechanical Industry and Research Institute of Energy Technology, "Study Report on Novel Dry DeSOx/DeNOx Technology for Cleaning Combustion Gases from Utility Boilers Using Pulse Corona Induced Plasma Chemical Process—PPCP," *Committee Reports*, No. 2EP-18 (1991).

Kawamura, K., "Simultaneous Removal of NOx and SOx by Electron Beam," *Kagaku Kogaku*, **53**, 820 (1989).

Kohl, A. L., and F. C. Riesenfeld, *Gas Purification*, 3rd ed., Gulf Pub., Houston (1979).

Löffler, F., *Staubabscheiden*, Thieme Verlag, Stuttgart (1988).

Massay, S. H., *Negative Ions*, Cambridge Univ. Press, Cambridge, England (1976).

Massay, S. H., *Atomic and Molecular Collisions*, Taylor & Francis, London (1979).

Masuda, S., "Pulse Corona Induced Plasma Chemical Process—A Horizon of New Plasma Chemical Technologies," *Proc. 8th Int. Symp. on Plasma Chemistry*, Tokyo, p. 2187 (1987).

Masuda, S., Y. Wu, T. Urabe, and Y. Ono, "Pulse Corona Induced Plasma Chemical Process for DeNox, DeSOx, and Mercury Vapour Control of Combustion Gas," *Proc. Int. Conf. on Electrostatic Precipitation*, Padova, Italy, p. 667 (1987).

Masuda, S., "Control of Air Toxic Material by Novel Plasma Chemical Process—PPCP and SPCP," *Proc. EPRI Symp. on Managing Hazardous Air Pollutants: State of the Art*, Washington, DC (1991).

Murakami, T., "Methods for Determination of Fluorine Compounds in Exhaust Gas," Japanese Industry Standard, K 0105 (1982).

Ogawa, A., *Separation of Particles from Air and Gases*, Vol. II, CRC Press, Boca Raton, FL (1984).

Tamon, H., H. Yano, and M. Okazaki, "A New Method of Gas Mixture Separation Based on Selective Electron Attachment," *Kagaku Kogaku Ronbunshu*, **15**, 663 (1989).

White, H. J., *Industrial Electrostatic Precipitation*, Addison-Wesley, London (1963).

Yabe, A., Y. Mori, and K. Hijikata, "EHD Study of the Corona Wind between Wire and Plate Electrode," *AIAA J.*, **16**, 340 (1978).

Yamamoto, T., and H. R. Velkoff, "Electrohydrodynamics in an Electrostatic Precipitator," *J. Fluid Mech.*, **108**, 1 (1981).

Manuscript received Sept. 12, 1994.